

Group-wise Sparse and Explainable Adversarial Attacks

Shpresim Sadiku*

*Zuse Institute Berlin & Technische Universität Berlin
Berlin, Germany*

sadiku@zib.de

Moritz Wagner*

*Zuse Institute Berlin & Technische Universität Berlin
Berlin, Germany*

wagner@zib.de

Sebastian Pokutta

*Zuse Institute Berlin & Technische Universität Berlin
Berlin, Germany*

pokutta@zib.de

Abstract

Sparse adversarial attacks fool deep neural networks (DNNs) through minimal pixel perturbations, typically regularized by the ℓ_0 norm. Recent efforts have replaced this norm with a structural sparsity regularizer, such as the nuclear group norm, to craft group-wise sparse adversarial attacks. The resulting perturbations are thus explainable and hold significant practical relevance, shedding light on an even greater vulnerability of DNNs than previously anticipated. However, crafting such attacks poses an optimization challenge, as it involves computing norms for groups of pixels within a non-convex objective. In this paper, we tackle this challenge by presenting an algorithm that simultaneously generates group-wise sparse attacks within semantically meaningful areas of an image. In each iteration, the core operation of our algorithm involves the optimization of a quasinorm adversarial loss. This optimization is achieved by employing the $1/2$ -quasinorm proximal operator for some iterations, a method tailored for nonconvex programming. Subsequently, the algorithm transitions to a projected Nesterov’s accelerated gradient descent with 2-norm regularization applied to perturbation magnitudes. We rigorously evaluate the efficacy of our novel attack in both targeted and non-targeted attack scenarios, on CIFAR-10 and ImageNet datasets. When compared to state-of-the-art methods, our attack consistently results in a remarkable increase in group-wise sparsity, e.g., an increase of 48.12% on CIFAR-10 and 40.78% on ImageNet (average case, targeted attack), all while maintaining lower perturbation magnitudes. Notably, this performance is complemented by a significantly faster computation time and a 100% attack success rate.

1 Introduction

Deep neural networks (DNNs) have exhibited vulnerability to adversarial attacks [CW17; Ath+18; Zho+20; Zha+20]. These attacks involve the deliberate introduction of perturbations into their inputs, effectively deceiving the network into generating incorrect predictions. Adversarial attacks raise significant security concerns for real-world systems and prompt inquiries into the generalization capabilities of neural classifiers [SHS19]. Simultaneously, investigating and harnessing adversarial attacks can serve as a valuable tool for diagnosing and ultimately fortifying the vulnerabilities of a DNN, notably through techniques such as adversarial training [Mad+18] or randomized smoothing [Yan+20].

While many methods for crafting adversarial examples focus on ℓ_p neighbourhoods with $p \geq 1$, recent research has explored the intriguing case of $p = 0$, leading to sparse adversarial attacks. The prevailing approaches for generating sparse adversarial attacks involve solving ℓ_0 -formulated problems, employing greedy

*Equal contribution.

single-pixel selection [SVS19], local search techniques [NK16], utilizing evolutionary algorithms [CH19], or relaxing ℓ_0 via the ℓ_1 ball and applying various algorithms to handle these structures [CW17; MMF19]. However, most of these methods only minimize the number of modified pixels and do not constrain the magnitude of the changed pixels. The perturbed pixels can thus exhibit substantial variations in intensity or colour compared to their surroundings, rendering them easily visible [SVS19]. This has motivated the generation of adversarial attacks that are simultaneously sparse and imperceptible [ZCW21; Imt+22]. Moreover, [Xu+19] and [KKW23] pinpoint the necessity of imposing structure to sparse adversarial attacks by generating group-wise sparse perturbations that are targeted to the main objective in the image. This way the generated perturbations are also explainable, i.e., they perturb semantically meaningful pixels in the images. Fig. 1 illustrates successful group-wise sparse adversarial examples generated by our proposed algorithm (GSE). In summary, the exploration of group-wise sparse and explainable adversarial attacks has evolved into a highly practical and relevant area of research. This line of research illuminates an even more significant vulnerability of DNNs than conventionally conceived, while also offering valuable insights for interpreting DNN failures, as discussed in [Xu+19]. Our main contributions are the following.

1. We establish a novel optimization framework that combines non-convex regularization with Nesterov’s accelerated gradient descent (NAG) procedure to craft adversarial attacks that are group-wise sparse. Our algorithmic foundation stems from an inventive fusion of the proximal gradient method outlined in [Tyr70] with a novel technique to increase the likelihood of perturbing pixels that are close to the already perturbed pixels.
2. Experiments conducted on the CIFAR-10 and NIPS2017 datasets underscore the superiority of our GSE (Group-wise Sparse and Explainable) attacks. In both targeted and untargeted attack scenarios, we surpass state-of-the-art methods, by requiring significantly fewer perturbations. For instance, we achieve a group-wise sparsity increase of 48.12% on CIFAR-10 and an impressive 40.78% increase on NIPS2017 (average case, targeted attack), all while maintaining smaller perturbation magnitudes and a remarkable 100% attack success rate.
3. Through a quantitative assessment of the alignment between perturbations and salient image regions, we underscore the value of GSE for interpretability analysis.

1.1 Related Work

Recent works have introduced methods for generating group-wise sparse and explainable adversarial attacks. StrAttack [Xu+19] represents a structured sparse and explainable adversarial attack, relying on the alternating direction method of multipliers (ADMM). It enforces group-wise sparsity through a dynamic sliding mask designed to extract spatial structures from the image. FWnucl-group [KKW23], which we will abbreviate as FWnucl, is another structured sparse adversarial attack. It quantifies the perturbation’s proximity to benign images by utilizing the nuclear group norm, capitalizing on the convexity of nuclear group norm balls through the application of a Frank-Wolfe optimization scheme [FW56]. Homotopy-Attack [ZCW21] is a sparse adversarial attack that operates based on the non-monotone accelerated proximal gradient algorithm (nmAPG) [LL15]. It can be extended to incorporate group-wise sparsity regularization by segmenting the image pixels using the SLIC superpixel algorithm and applying regularization using the resulting 2,0-“norm”. SAIF [Imt+22] is an attack method that achieves sparsity and explainability. It employs the Frank-Wolfe algorithm [FW56] for the joint optimization of the perturbation and a sparsity mask. We empirically compare our approach to the aforementioned attacks.

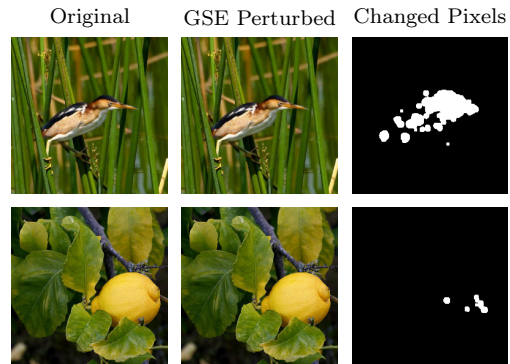


Figure 1: Adversarial examples generated by our algorithm. The first row depicts a targeted attack with the target label “water bottle”, and the second row depicts an untargeted attack.

Interpretability. A recent research area involves the integration of adversarial examples and model explanations, emphasizing the convergence of fundamental concepts in both domains. On simple datasets like MNIST, [INM19] illustrates a hitting set duality between model explanations and adversarial examples. Another study shows the correspondence of attack perturbations with discriminative image features [Xu+19]. Our attack strategy involves perturbing regions neighbouring already perturbed pixels. Since we start with very sparse perturbations this results in a change of the most susceptible pixels of an image. In addition, we conduct empirical analysis to examine the overlap between our attacks and salient image regions. For the quantitative interpretability analysis we make use of the adversarial saliency map [Pap+16; Xu+19] while for the visual analysis, we employ a class activation map as proposed in [Zho+16].

2 Method

2.1 Problem Formulation

Consider $\mathcal{X} = [I_{\min}, I_{\max}]^{M \times N \times C}$, which represents a set of feasible images. Here, M and N stand for the height and width of the image, while C denotes the number of colour channels. Let $\mathbf{x} \in \mathcal{X}$ be a benign image with label $l \in \mathbb{N}$, and $t \in \mathbb{N}$ be a target label, where $t \neq l$. Additionally, let $\mathcal{L} : \mathcal{X} \times \mathbb{N} \rightarrow \mathbb{R}$ be a classification loss function, such as the cross-entropy loss, tailored for a given classifier \mathcal{C} . For the sake of simplicity, we assume \mathbf{x} is vectorized.

Moreover, we introduce a distortion function $\mathcal{D} : \mathbb{R}^{M \times N \times C} \rightarrow \mathbb{R}_{\geq 0}$. The goal of a *targeted adversarial attack* is to find an image \mathbf{x}_{adv} to which \mathcal{C} assigns the target label t and that is in close proximity to \mathbf{x} according to the function \mathcal{D} . In summary, the task of formulating a targeted adversarial example for the input \mathbf{x} can be framed as

$$\min_{\mathbf{w} \in \mathbb{R}^{M \times N \times C}} \mathcal{L}(\mathbf{x} + \mathbf{w}, t) + \lambda \mathcal{D}(\mathbf{w}), \quad (1)$$

where $\lambda > 0$. The targeted formulation of Eq. (1) can be adapted to generate *untargeted adversarial attacks* by maximizing the loss with respect to the true label l . Thus, in the untargeted scenario, we encounter the following problem

$$\min_{\mathbf{w} \in \mathbb{R}^{M \times N \times C}} -\mathcal{L}(\mathbf{x} + \mathbf{w}, l) + \lambda \mathcal{D}(\mathbf{w}).$$

However, in the subsequent section, we focus on the targeted attack setting.

2.2 Quasinorm Regularization

Targeted sparse adversarial examples can be crafted by solving the quasinorm-regularized problem [WYD21]

$$\min_{\mathbf{w} \in \mathbb{R}^{M \times N \times C}} \mathcal{L}(\mathbf{x} + \mathbf{w}, t) + \lambda \|\mathbf{w}\|_p^p, \quad (2)$$

for $0 < p < 1$. Here $\|\mathbf{w}\|_p = (\sum_i |w_i|^p)^{\frac{1}{p}}$ is only a quasinorm since subadditivity is not satisfied for $p < 1$. After successfully solving Eq. (2) and obtaining $\hat{\mathbf{w}} \in \arg \min_{\mathbf{w} \in \mathbb{R}^{M \times N \times C}} \mathcal{L}(\mathbf{x} + \mathbf{w}, t) + \lambda \|\mathbf{w}\|_p^p$, the resulting adversarial example can be expressed as

$$\mathbf{x}_{\text{adv}} = \text{clip}_{\mathcal{X}}(\mathbf{x} + \hat{\mathbf{w}}).$$

To obtain $\hat{\mathbf{w}}$, we apply the forward-backward splitting algorithm, as detailed in Algorithm 1. In their work, [CSX13] derive a closed-form solution for the proximal operator of $\|\cdot\|_p^p$

$$\text{prox}_{\lambda \|\cdot\|_p^p}(\mathbf{w}) := \arg \min_{\mathbf{y} \in \mathbb{R}^{M \times N \times C}} \frac{1}{2\lambda} \|\mathbf{y} - \mathbf{w}\|_2^2 + \|\mathbf{y}\|_p^p, \quad (3)$$

for $p = \frac{1}{2}$. Given that $\|\cdot\|_p^p$ is separable, by [Bec17, Theorem 6.6] it is sufficient to deduce the characterization of $\text{prox}_{\lambda \|\cdot\|_p^p}$ in Eq. (3) when $MNC = 1$. Each component is thus given by

$$\left[\text{prox}_{\lambda \|\cdot\|_p^p}(\mathbf{z}) \right]_i = \frac{2}{3} z_i \left(1 + \cos \left(\frac{2\pi}{3} - \frac{2\phi_{2\lambda} z_i}{3} \right) \right) \mathbb{1}_S(i), \quad (4)$$

Algorithm 1 Forward-Backward Splitting Attack

Require: Image $\mathbf{x} \in \mathcal{X}$, target label t , loss function \mathcal{L} , sparsity parameter $\lambda > 0$, step sizes α_k , number of iterations K .

- 1: Initialize $\mathbf{w}^{(0)} = \mathbf{0}$.
 - 2: **for** $k = 0, \dots, K - 1$ **do**
 - 2: $\mathbf{w}^{(k+1)} = \text{prox}_{\alpha_k \lambda \|\cdot\|_p^p}(\mathbf{w}^{(k)} - \alpha_k \nabla_{\mathbf{w}^{(k)}} \mathcal{L}(\mathbf{x} + \mathbf{w}^{(k)}, t))$
 - 3: **end for**
 - 4: **return** $\hat{\mathbf{w}} = \mathbf{w}^{(K)}$
-

where

$$\phi_{2\lambda} = \arccos\left(\frac{2\lambda}{8} \left(\frac{|z_i|}{3}\right)^{-\frac{3}{2}}\right),$$
$$g(2\lambda) = \frac{\sqrt[3]{54}}{4} (2\lambda)^{\frac{2}{3}}, S = \{i : |z_i| > g(2\lambda)\}.$$

2.3 Group-wise Sparsity

In this section, we propose a method for generating group-wise sparse adversarial examples while ensuring a small perturbation magnitude, with $\mathcal{D} = \|\cdot\|_2$ in Eq. (1). To induce group-wise sparsity in the perturbation vector \mathbf{w} , we apply the 1/2-quasinorm regularization to compute a subspace V within $\mathbb{R}^{M \times N \times C}$, which enforces group-wise sparsity as a constraint. To identify such a subspace, we use a vector of tradeoff parameters $\lambda \in \mathbb{R}_{\geq 0}^{M \times N \times C}$ for the 1/2-quasinorm regularization term, allowing us to adjust each entry individually. We reduce $\lambda_{i,j,:}$ for pixels located in proximity to already perturbed pixels, thereby making them more amenable to perturbation. This operation is denoted as $\text{prox}_{\lambda \|\cdot\|_p^p}(\mathbf{z})$. Due to Eq. (4), we can formally define

$$\left[\text{prox}_{\lambda \|\cdot\|_p^p}(\mathbf{z})\right]_i := \left[\text{prox}_{\lambda_i \|\cdot\|_p^p}(\mathbf{z})\right]_i,$$

for $\lambda \in \mathbb{R}_{\geq 0}^{M \times N \times C}$. Having computed an iterate $\mathbf{w}^{(k)}$ by forward-backward splitting with Nesterov momentum as shown in Algorithm 2, we adjust $\lambda^{(k)}$ as follows (`AdjustLambda` in Algorithm 2). First, we build a mask

$$\mathbf{m} = \text{sign}\left(\sum_{c=1}^C |\mathbf{w}^{(k)}|_{:, :, c}\right) \in \{0, 1\}^{M \times N}, \quad (5)$$

to identify perturbed pixels. Next, we perform a 2D convolution on \mathbf{m} using a square Gaussian blur kernel $\mathbf{K} \in \mathbb{R}^{n \times n}$ with appropriate padding, yielding a matrix

$$\mathbf{M} = \mathbf{m} * * \mathbf{K} \in [0, 1]^{M \times N},$$

where entries with indices close to non-zero entries in \mathbf{m} are non-zero. Assuming n is odd and setting $\hat{n} = \lfloor \frac{n}{2} \rfloor$ the convolution is defined as

$$[\mathbf{m} * * \mathbf{K}]_{i,j} = \sum_{k=-\hat{n}}^{\hat{n}} \sum_{l=-\hat{n}}^{\hat{n}} \mathbf{K}_{k+\hat{n}+1, l+\hat{n}+1} \cdot \mathbf{m}_{i+k, j+l}.$$

Our next step involves the build of a matrix $\overline{\mathbf{M}} \in \mathbb{R}^{M \times N}$ with

$$\overline{\mathbf{M}}_{ij} = \begin{cases} \mathbf{M}_{ij} + 1, & \text{if } \mathbf{M}_{ij} \neq 0, \\ q, & \text{else,} \end{cases}$$

where $0 < q \leq 1$. When $q < 1$, we increase the tradeoff parameters for pixels situated at a distance from those previously perturbed. Next, we compute the tradeoff parameters for the following iteration

$$\lambda_{i,j,:}^{(k+1)} = \frac{\lambda_{i,j,:}^{(k)}}{\overline{\mathbf{M}}_{i,j}}.$$

Algorithm 2 Group-Wise Sparse Attack

Require: Image $\mathbf{x} \in \mathcal{X}$, target label t , loss function \mathcal{L} , regularization parameters $\lambda, \mu > 0$, step size $\sigma > 0$, numbers of iterations \hat{k}, K , sequence α_k .

- 1: Initialize $\mathbf{w}^{(0)} = \mathbf{0}$, $\lambda^{(0)} = \lambda \mathbf{1}$
- 2: Define $f(\mathbf{w}) := \mathcal{L}(\mathbf{x} + \mathbf{w}, t) + \mu \|\mathbf{w}\|_2$
- 3: **for** $k = 0, \dots, \hat{k} - 1$ **do**
- 3: $\tilde{\mathbf{w}}^{(k+1)} = \text{prox}_{\sigma \lambda^{(k)} \|\cdot\|_p} (\mathbf{w}^{(k)} - \sigma \nabla_{\mathbf{w}^{(k)}} (f(\mathbf{w}^{(k)})))$
- 3: $\mathbf{w}^{(k+1)} = (1 - \alpha_k) \tilde{\mathbf{w}}^{(k+1)} + \alpha_k \tilde{\mathbf{w}}^{(k)}$
- 3: $\lambda^{(k+1)} = \text{AdjustLambda}(\lambda^{(k)}, \mathbf{w}^{(k+1)})$
- 4: **end for**
- 5: **for** $k = \hat{k}, \dots, K - 1$ **do**
- 5: $\tilde{\mathbf{w}}^{(k+1)} = \mathbf{w}^{(k)} - \sigma \nabla_{\mathbf{w}^{(k)}} (f(\mathbf{w}^{(k)}))$
- 5: $\mathbf{w}^{(k+1)} = P_V ((1 - \alpha_k) \tilde{\mathbf{w}}^{(k+1)} + \alpha_k \tilde{\mathbf{w}}^{(k)})$
- 6: **end for**
- 7: **return** $\hat{\mathbf{w}} = \mathbf{w}^{(K)}$

In this manner, we expand regions with lower tradeoff parameters over a specified \hat{k} iterations. It is crucial to highlight that our method operates independently of predefined structures, such as pixel partitions. In all subsequent iterations, we employ projected NAG to approximate a solution to a simplified problem

$$\min_{\mathbf{w} \in V} \mathcal{L}(\mathbf{x} + \mathbf{w}, t) + \mu \|\mathbf{w}\|_2, \quad (6)$$

where $\mu > 0$ serves as a tradeoff parameter and

$$V := \text{span}(\{e_{i,j,c} \mid \lambda_{i,j,c}^{(\hat{k})} < \lambda_{i,j,c}^{(0)}\}) \subseteq \mathbb{R}^{M \times N \times C},$$

is a subspace spanned by standard unit vectors $e_{i,j,c}$. As V is spanned by these standard unit vectors, we can express the projection onto V as

$$[P_V(\mathbf{w})]_{i,j,c} = \begin{cases} \mathbf{w}_{i,j,c}, & \text{if } e_{i,j,c} \in V, \\ 0, & \text{otherwise.} \end{cases}$$

In the following iterations, perturbations will only affect pixels at coordinates (i, j) with tradeoff parameters $\lambda_{i,j,c}^{(\hat{k})}$ below the initial λ . Due to Eq. (5), it follows that $e_{i,j,c} \in V$ for all channels c of a perturbed pixel at (i, j) , meaning most often all channels of the pixel will be perturbed. This process is succinctly outlined in Algorithm 2, where we introduce the sequence α_k as described in [Nes83]

$$\beta_0 = 0, \quad \beta_k = \frac{1 + \sqrt{1 + 4\beta_{k-1}^2}}{2}, \quad \alpha_k = \frac{1 - \beta_k}{\beta_{k+1}}.$$

In our tests, we initially perform a section search to find the maximum λ where $\tilde{\mathbf{w}}^{(1)} \neq \mathbf{0}$. Subsequently, we conduct another section search to determine the appropriate λ at which the attack succeeds.

2.4 Equivalence to NAG of unconstrained problems

Consider $d = MNC$, where our image $\mathbf{x} \in [I_{\min}, I_{\max}]^d$ is vectorized. Let \mathcal{I} denote the set that encompasses indices corresponding to entries with $\lambda_{i,j,c}^{(\hat{k})} \geq \lambda_{i,j,c}^{(0)}$ after \hat{k} iterations. Also, let $m := |\mathcal{I}| < d$. With these considerations, we can formulate the optimization problem in Eq. (6), which arises following iteration \hat{k} , as

$$\begin{aligned} \min_{\mathbf{w}} \quad & \mathcal{L}(\mathbf{x} + \mathbf{w}, t) + \mu \|\mathbf{w}\|_2 \\ \text{s.t.} \quad & A\mathbf{w} = 0, \end{aligned} \quad (7)$$

where $A \in \{0, 1\}^{m \times d}$ has rows

$$\left(\underbrace{0, \dots, 0}_{i-1 \text{ times}}, 1, \underbrace{0, \dots, 0}_{d-i \text{ times}} \right), \quad \forall i \in \mathcal{I}. \quad (8)$$

We can eliminate the equality constraints using the nullspace method. Let $H \in \mathbb{R}^{d \times d}$ be an orthogonal matrix and $R \in \mathbb{R}^{m \times m}$ an upper triangular matrix, obtained by QR-decomposition of A^\top , i.e.,

$$HA^\top = \begin{pmatrix} R \\ 0 \end{pmatrix}. \quad (9)$$

Further let $H = (Y, Z)^\top$, where $Y^\top \in \mathbb{R}^{m \times d}$ contains the first m rows of H and $Z \in \mathbb{R}^{d \times d-m}$. Because an orthogonal matrix H possesses full rank, both Y and Z also exhibit full rank. Hence we can uniquely write any $\mathbf{w} \in \mathbb{R}^d$ as

$$\mathbf{w} = Y\mathbf{w}_y + Z\mathbf{w}_z = H^\top \begin{pmatrix} \mathbf{w}_y \\ \mathbf{w}_z \end{pmatrix},$$

with $\mathbf{w}_y \in \mathbb{R}^m, \mathbf{w}_z \in \mathbb{R}^{d-m}$. In particular, for any $\mathbf{w} \in \ker A$ we have

$$0 = A\mathbf{w} = AH^\top \begin{pmatrix} \mathbf{w}_y \\ \mathbf{w}_z \end{pmatrix} = (R^\top, 0) \begin{pmatrix} \mathbf{w}_y \\ \mathbf{w}_z \end{pmatrix} = R^\top \mathbf{w}_y.$$

Given Eqs. (8) and (9), we can establish that both A and R possess rank m . Consequently, we can represent any $\mathbf{w} \in \ker A$ as $Z\mathbf{w}_z$, where $\mathbf{w}_z \in \mathbb{R}^{d-m}$. This allows us to formulate an unconstrained problem equivalent to Eq. (7)

$$\min_{\mathbf{z} \in \mathbb{R}^{d-m}} \mathcal{L}(\mathbf{x} + Z\mathbf{z}, t) + \mu \|Z\mathbf{z}\|_2. \quad (10)$$

Setting $f(\mathbf{w}) = \mathcal{L}(\mathbf{x} + \mathbf{w}, t) + \mu \|\mathbf{w}\|_2$ and $F(\mathbf{z}) = f(Z\mathbf{z})$ we get from the update step of NAG

$$\begin{aligned} \mathbf{w}_{k+1} &= Z\mathbf{z}_{k+1} \\ &= Z \left((1 - \alpha_k) \left(\mathbf{z}^{(k)} - \sigma \nabla F(\mathbf{z}^{(k)}) \right) + \alpha_k \left(\mathbf{z}^{(k-1)} - \sigma \nabla F(\mathbf{z}^{(k-1)}) \right) \right) \\ &= (1 - \alpha_k) \left(\mathbf{w}^{(k)} - \sigma ZZ^\top \nabla f(\mathbf{w}^{(k)}) \right) + \alpha_k \left(\mathbf{w}^{(k-1)} - \sigma ZZ^\top \nabla f(\mathbf{w}^{(k-1)}) \right) \\ &= (1 - \alpha_k) \left(\mathbf{w}^{(k)} - \sigma P_V(\nabla f(\mathbf{w}^{(k)})) \right) + \alpha_k \left(\mathbf{w}^{(k-1)} - \sigma P_V(\nabla f(\mathbf{w}^{(k-1)})) \right) \\ &= P_V \left((1 - \alpha_k) \left(\mathbf{w}^{(k)} - \sigma \nabla f(\mathbf{w}^{(k)}) \right) + \alpha_k \left(\mathbf{w}^{(k-1)} - \sigma \nabla f(\mathbf{w}^{(k-1)}) \right) \right), \end{aligned}$$

where the last equality holds since $\mathbf{w}^{(k)}, \mathbf{w}^{(k-1)} \in V$. Hence the projected NAG in Algorithm 2 has the same properties as NAG solving the unconstrained problem in Eq. (10), and thus converges as such.

3 Experiments

We now demonstrate the effectiveness of our proposed GSE attack for crafting group-wise sparse adversarial attacks. Secs. 3.1 and 3.2 outline our experimental setups and define the relevant comparing metrics, while Secs. 3.3.1 and 3.3.2 systematically compare our approach with multiple previous state-of-the-art (SOTA) group-wise sparse adversarial attacks, including FWnucl [KKW23], Homotopy-Attack [ZCW21], and StrAttack [Xu+19]. Additionally, Secs. 3.3.3 to 3.3.5 cover ablation studies regarding the explainability of our group-wise sparse attacks, visualizations, and empirical time costs.

3.1 Setup

We run comprehensive experiments on the NIPS2017* and CIFAR-10 [KH+09] datasets. NIPS2017 consists of 1,000 images of size $299 \times 299 \times 3$ on which we test the attacks against a ResNet50 [He+16] and a VGG19 [SZ15] ImageNet classifier. CIFAR-10 comprises images of size $32 \times 32 \times 3$ and is split into a training set consisting of 50,000 images, where we train a ResNet20 classifier [He+16]. Additionally, there is a test set comprising 10,000 images on which we perform our experiments. In our attack configuration, we fix the Gaussian blur kernel size at 5 for both datasets. Specifically, for CIFAR-10, we set $q = 0.25$, $\sigma = 0.0025$, $\mu = 1$, and $\hat{k} = 30$, while for NIPS2017, we configure it with $q = 0.9$, $\sigma = 0.025$, $\mu = 0.1$, and $\hat{k} = 50$. Regarding StrAttack, we modify the authors’ implementation to be compatible with the PyTorch framework, employing the parameters recommended in [Xu+19], specifically those from Appendix F. For FWnucl, we develop an implementation for the nuclear group norm attack using PyTorch, setting $\varepsilon = 5$. We run all three attacks for a total of 200 iterations. For the Homotopy-Attack, we adjust the authors’ implementation to support group-wise sparsity, as outlined in [ZCW21], and we follow their recommended parameter settings. All tests are run on a machine with an NVIDIA Tesla T4 GPU. Our codes are available at <https://github.com/wagnermoritz/GSE>.

3.2 Evaluation

Consider a set of n images $(\mathbf{x}^{(i)})_{0 < i \leq n}$ and the corresponding perturbations $(\delta^{(i)})_{0 < i \leq n}$, where $\mathbf{x}^{(i)}, \mathbf{x}^{(i)} + \delta^{(i)} \in \mathcal{X}$. Among these, let $m \leq n$ denote the number of successfully generated adversarial examples $\mathbf{x}^{(i)} + \delta^{(i)}$. We define the attack success rate (ASR) as

$$\text{ASR} = \frac{m}{n},$$

and the average number of changed pixels (ACP) via

$$\text{ACP} = \frac{1}{n} \sum_{i=1}^n \frac{\|\Delta^{(i)}\|_0}{MN}, \quad \Delta^{(i)} = \sum_{c=1}^C |\delta_{[:, :, c]}^{(i)}| \in \mathbb{R}^{M \times N}.$$

We determine the number of perturbed pixel clusters in $\mathbf{x}^{(i)} + \delta^{(i)}$ by creating a mask

$$\mathbf{m}^{(i)} = \text{sign} \left(\sum_{c=1}^C |\delta_{[:, :, c]}^{(i)}| \right) \in \{0, 1\}^{M \times N},$$

and then running depth-first search (DFS) on that mask, treating adjacent 1-entries as neighbouring nodes. We rerun DFS starting from every 1-entry that another DFS run has not yet discovered. The number of DFS runs until all 1-entries are discovered is the number of clusters. Finally, we compute the average number of clusters (ANC) for our m adversarial examples.

Now, consider $\mathbf{x} \in [I_{\min}, I_{\max}]^d$ as a vectorized image and let $Z(\mathbf{x})$ represent the logits of a classifier. The *adversarial saliency map (ASM)* [Pap+16; Xu+19] is defined as follows

$$\text{ASM}(\mathbf{x}, t)[i] = \left(\frac{\partial Z(\mathbf{x})_t}{\partial \mathbf{x}_i} \right) \left| \frac{\partial Z(\mathbf{x})_l}{\partial \mathbf{x}_i} \right| \mathbb{1}_S(i),$$

$$S = \left\{ i \in \{1, \dots, d\} \mid \frac{\partial Z(\mathbf{x})_t}{\partial \mathbf{x}_i} \geq 0 \text{ or } \frac{\partial Z(\mathbf{x})_l}{\partial \mathbf{x}_i} \leq 0 \right\}.$$

The metric $\text{ASM}(\mathbf{x}, t) \in \mathbb{R}_{\geq 0}^d$ provides a measure of importance for each pixel. It is worth noting that a higher ASM value signifies greater pixel significance. We compute a binary mask $\mathbf{B}_{ASM} \in \{0, 1\}^d$ by

$$\mathbf{B}_{ASM}[i] = \begin{cases} 1, & \text{if } \text{ASM}(\mathbf{x}, t)[i] > \nu, \\ 0, & \text{otherwise,} \end{cases}$$

*<https://www.kaggle.com/competitions/nips-2017-defense-against-adversarial-attack/data>

	Attack	ASR	ACP	ANC	ℓ_2	$d_{2,0}$	Time
Untargeted	GSE (Ours)	100%	38.0	1.6	0.71	178	9.9s
	Homotopy	100%	72.5	2.5	0.64	253	1751s
Targeted	GSE (Ours)	100%	96.9	2.4	1.28	300	11.8s
	Homotopy	100%	104	3.7	1.22	371	1812s

Table 1: Comparison of our attack and the Homotopy-Attack on a ResNet20 classifier for CIFAR-10. The perturbations for both attacks were computed for all images sequentially. Due to the extensive computation time required by the Homotopy-Attack, we tested on a limited sample size of 100.

where ν is some percentile of the entries of $\text{ASM}(\mathbf{x}, t)$. Given an adversarial perturbation $\delta \in \mathbb{R}^d$, we can now compute the interpretability score (IS) as

$$\text{IS}(\delta) = \frac{\|\mathbf{B}_{ASM} \odot \delta\|_2}{\|\delta\|_2}.$$

Note that when $\text{IS}(\delta)$ approaches 1, the perturbation primarily targets pixels crucial for the class prediction of the model. Conversely, IS scores nearing zero do not lend themselves to meaningful interpretation based on ASM scores. Let \mathcal{C} be a convolutional neural network classifier and $f_k[i, j]$ be the activation of the unit k at the coordinates (i, j) in the last convolutional layer of \mathcal{C} evaluated at \mathbf{x} . Then, using global average pooling after the last convolutional layer, the input to the softmax corresponding to label l is

$$\sum_k w_k^l \sum_{i,j} f_k[i, j] = \sum_{i,j} \sum_k w_k^l f_k[i, j],$$

where w_k^l are the weights corresponding to the label l for unit k . Since w_k^l indicate the importance of $\sum_{i,j} f_k[i, j]$ for class l , the *class activation map (CAM)* [Zho+16] is defined by

$$\text{CAM}_l[i, j] = \sum_k w_k^l f_k[i, j],$$

and directly indicates the importance of activation at (i, j) for the classification of \mathbf{x} as class l . To make the comparison of CAM_l and \mathbf{x} easier, the resulting class activation map is upscaled to the size of \mathbf{x} using bicubic interpolation. The value $\|\delta\|_{2,0}$ for a perturbation δ , as proposed in [ZCW21], heavily depends on the pixel partitioning method. To measure the group-wise sparsity of a perturbation, we propose a function that considers all n by n pixel patches of an image instead of only a subset that results in a partition. In our experiments, we set $n = 8$. Let $\delta \in \mathbb{R}^{M \times N \times C}$, $n < M, N$, and let $\mathcal{G} = \{G_1, \dots, G_k\}$ be a set containing the index sets of all overlapping n by n patches in δ . Then we define

$$d_{2,0}(\delta) := |\{i : \|\delta_{G_i}\|_2 \neq 0, i = 1, \dots, k\}|.$$

We evaluate all attacks on these metrics in the untargeted and in the targeted setting. For CIFAR-10, the targeted attacks are performed with respect to each wrong label. For the evaluation of the attacks on ImageNet models, we choose ten target labels for each image by randomly choosing ten distinct numbers $a_1, \dots, a_{10} \in \{1, \dots, 999\}$ and defining the target labels t_i for an image with the true label l by $t_i = l + a_i \bmod 1000$. In the targeted setting, as suggested in [Fan+20], we give three versions of each metric: best, average, and worst case. For the best and worst case, we take the best and worst results, respectively, obtained from the targeted attacks for each image. For the average case, we take the mean of all results.

3.3 Results

As evidenced in Tab. 1, our method significantly outperforms the Homotopy-Attack [ZCW21] in both targeted and untargeted attacks on CIFAR-10. It is worth noting that the only metric where Homotopy-Attack surpasses our method is the 2-norm perturbation magnitude. However, this metric is of secondary importance in the group-wise sparse attack setting. In contrast, our method excels in achieving an increase in overall sparsity and group-wise sparsity, all while substantially reducing the cluster count and the computation time by two orders of magnitude. Hence, we will exclude Homotopy-Attack from our subsequent experiments.

	Attack	ASR	ACP	ANC	ℓ_2	$d_{2,0}$
CIFAR-10 ResNet20	GSE (Ours)	100%	36.8	1.5	0.75	177
	StrAttack	100%	117	4.7	1.07	419
	FWnucl	95.1%	456	1.3	2.00	592
NIPS2017 VGG19	GSE (Ours)	100%	968	6.7	1.25	2596
	StrAttack	100%	4021	7.4	1.92	7058
	FWnucl	89.1%	7225	2.1	2.40	7985
NIPS2017 ResNet50	GSE (Ours)	100%	1270	8.2	1.47	2922
	StrAttack	100%	8669	12.9	2.51	13963
	FWnucl	48.6%	14953	3.7	1.82	17083

Table 2: Untargeted attacks performed on a ResNet20 classifier for CIFAR-10, a VGG19 and a ResNet50 classifier for ImageNet/NIPS2017. Tested on 1,000 samples from each dataset.

Dataset	Attack	Best case					Average case					Worst case				
		ASR	ACP	ANC	ℓ_2	$d_{2,0}$	ASR	ACP	ANC	ℓ_2	$d_{2,0}$	ASR	ACP	ANC	ℓ_2	$d_{2,0}$
CIFAR-10 ResNet20	GSE (Ours)	100%	29.6	1.2	0.69	151	100%	80.1	2.1	1.17	276	100%	148	3.5	1.62	413
	StrAttack	100%	75.4	2.2	0.79	336	100%	232	5.4	1.96	532	100%	430	9.0	4.72	620
	FWnucl	100%	276	1.0	1.44	504	82.8%	384	1.6	2.32	567	35.0%	471	2.8	3.78	602
NIPS2017 VGG19	GSE (Ours)	100%	1974	4.9	2.72	3695	100%	6025	10.5	3.58	9704	100%	15996	17.2	4.39	21489
	StrAttack	100%	3616	3.6	2.85	5863	100%	10940	11.0	3.70	16545	100%	23245	19.9	5.48	32193
	FWnucl	56.1%	4489	1.3	2.91	5783	18.3%	7133	1.9	3.92	11639	0.0%	N/A	N/A	N/A	N/A
NIPS2017 ResNet50	GSE (Ours)	100%	2090	3.8	2.51	3498	100%	7311	9.5	3.15	10734	100%	16284	15.9	3.65	21872
	StrAttack	100%	6117	4.0	2.73	9246	100%	15308	12.1	4.17	21182	100%	26569	20.5	7.88	33297
	FWnucl	32.4%	9897	3.4	2.82	11134	12.6%	11735	6.3	3.96	18126	0.0%	N/A	N/A	N/A	N/A

Table 3: Targeted attacks performed on a ResNet20 classifier for CIFAR-10, a VGG19 and a ResNet50 classifier for ImageNet/NIPS2017. Tested on 1,000 samples from each dataset.

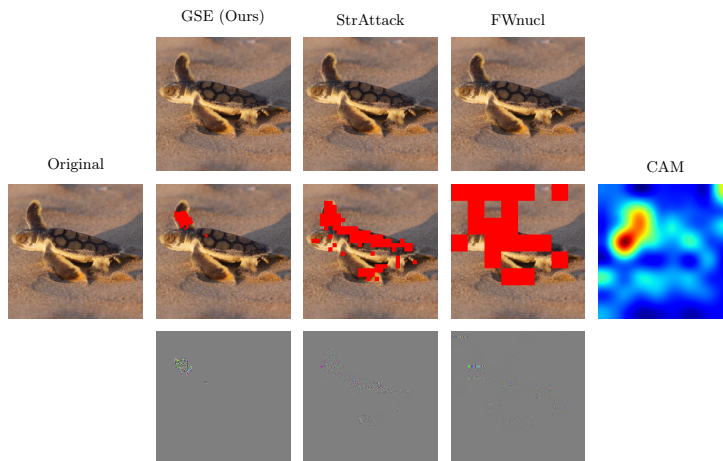


Figure 2: Visual comparison of successful untargeted adversarial instances generated by our attack, StrAttack, and FWnucl. Adversarial examples are shown in the top row, perturbed pixels highlighted in red in the middle row, and the perturbations in the bottom row. The target model is a ResNet50. The perturbations are enhanced for visibility.

3.3.1 Untargeted Attack

Tab. 2 displays the results of untargeted attacks on CIFAR-10 and NIPS2017 datasets. Notably, our method and StrAttack attain a 100% ASR in both cases. Furthermore, our algorithm significantly outperforms other attacks in terms of ACP. Specifically, on average, our algorithm achieves 3.6% sparsity on CIFAR-10 images and 1.5% on NIPS2017 images when attacking a VGG19 classifier. The only metric where other SOTA methods outperform GSE is the ANC. Nevertheless, this advantage remains insignificant when considering the considerably lower values of ACP achieved by our method. Furthermore, as observed from the $d_{2,0}$ metric, our method attains an exceptionally high level of group-wise sparsity. To be precise, we attain a remarkable increase of group-wise sparsity by 57.76% on CIFAR-10 and 63.22% on NIPS2017 when attacking a VGG19 classifier, in comparison to the SOTA. Notably, we accomplish this while preserving the minimal magnitude of attacks, as measured by the 2-norm. To further substantiate the effectiveness of our method on the NIPS2017 dataset, we replicate the previous experiments with a stronger backbone classifier - ResNet50. The results in Tab. 2 demonstrate that our algorithm surpasses SOTA by a substantial margin. Specifically, our algorithm achieves a remarkable increase of 85.35% in sparsity and 79.08% in group-wise sparsity, while also attaining the lowest perturbation norm.

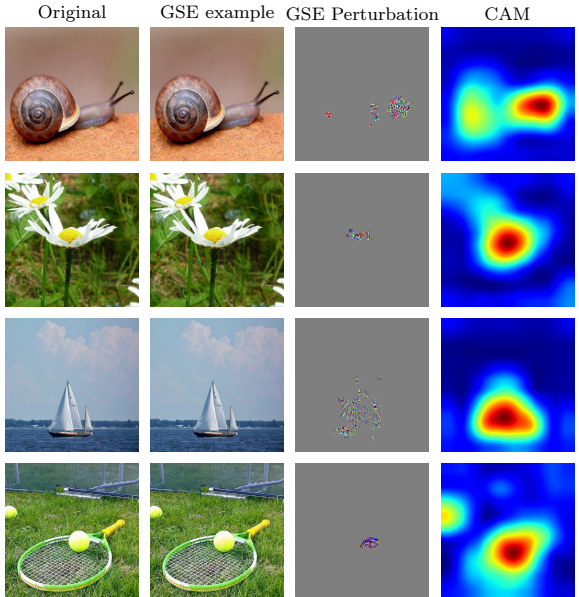


Figure 3: Targeted adversarial examples generated by GSE. The target is “airship” for the first two rows, and “golf cart” for the last two rows. The attacked model is a VGG19. The perturbations are enhanced for visibility.

3.3.2 Targeted Attack

The results for targeted attacks on CIFAR-10 and NIPS2017 datasets are presented in Tab. 3. While our method and StrAttack attain a perfect ASR in both cases, FWnucl results in a 0% worst-case ASR on the NIPS2017 dataset. This implies that for every tested NIPS2017 image, the worst-case target label results in an unsuccessful FWnucl attack, consequently yielding no values for FWnucl’s worst-case metrics. When examining the ACP, it becomes evident that our algorithm yields the sparsest perturbations, changing on average only 7.8% of the pixels in the CIFAR-10 images and a mere 9.2% (11.2%) of the pixels in the NIPS2017 images when attacking a VGG10 (ResNet50) classifier. Moreover, it is clear from the $d_{2,0}$ metric that our method achieves a remarkable group-wise sparsity. On average, we demonstrate a significant decrease of $d_{2,0}$ by 48.13% on CIFAR-10 and 16.63% (40.78%) on NIPS2017 when attacking a VGG19 (ResNet50) classifier, while still having the lowest magnitude of the attacks, measured by the 2-norm. Similarly to Sec. 3.3.1, the only metric other SOTA methods outperform GSE is the number of clusters. However, this is still insignificant considering, amongst others, the high ACP as well as the low ASR compared to our method.

3.3.3 Visualization

We display the visualizations for untargeted group-wise sparse adversarial examples in Fig. 2, while Fig. 3 presents those for targeted group-wise sparse adversarial examples. Using the CAM technique [Zho+16], we demonstrate the alignment between our algorithm’s perturbations and localized, class-specific discriminative regions within the images. Clearly, the generated perturbations effectively encompass the most discriminative areas of the objects, a testament to our algorithm’s impressive achievement of interpretability.

Attack	Untargeted			Targeted		
	CIFAR-10	ImageNet		CIFAR-10	ImageNet	
	ResNet20	ResNet50	VGG19	ResNet20	ResNet50	VGG19
GSE (Ours)	0.39s	23.8s	38.9s	0.39s	20.1s	40.8s
StrAttack	1.33s	48.9s	78.2s	1.28s	49.2s	75.5s
FWnucl	0.80s	32.4s	67.1s	0.82s	31.9s	65.8s

Table 4: Comparison of empirical attack computation time per image. In every experiment, all attacks utilize the same batch size.

3.3.4 Interpretability Evaluation

Fig. 4 illustrates the IS metric for the targeted attacks across various percentiles of ASM scores for samples from the CIFAR-10 and NIPS2017 datasets. Notably, the figure highlights that our method consistently achieves higher IS scores compared to other group-wise sparse attacks, especially for higher percentiles ν . This shows that the perturbations generated by GSE are more focused on the most salient regions of the image. In addition, we have incorporated the recently proposed SAIF method [Imt+22], which aims to establish a strong correlation between the generated perturbations and the salient regions within an image. SAIF surpasses our attack on the NIPS2017 dataset, specifically for percentiles at or above the 80th. This advantage may be attributed, in part, to SAIF’s lack of group-wise sparsity, allowing it to have greater overlap with the non-group-wise sparse ASM at higher percentiles. We omitted SAIF from our previous tables due to its poor group-wise sparse nature.

3.3.5 Speed Comparison

In this section, we conduct a runtime comparison between our algorithm and SOTA methods, with the results summarized in Tab. 4. Notably, our algorithm demonstrates significantly faster performance compared to FWnucl [KKW23] and StrAttack [Xu+19]. This speed advantage stems partially from the method used to enforce group-wise sparsity. StrAttack calculates the Euclidean norm of each group of pixels in every iteration and integrates this outcome as regularization using ADMM. FWnucl, on the other hand, computes a solution for a nuclear group-norm LMO in each iteration. In contrast, our attack initially computes a solution for the $1/2$ -quasinorm proximal operator in the first \hat{k} iterations. Subsequently, the attack transitions to projected NAG with 2-norm regularization, which is less computationally costly than the methods employed by both StrAttack and FWnucl.

4 Conclusion

In this paper, we introduced “GSE”, a novel algorithm for generating group-wise sparse and explainable adversarial attacks. Our approach is rooted in proximal gradient methods for non-convex programming, featuring additional control over changed pixels, and the use of projected NAG technique to solve optimization problems. Extensive experiments validate that GSE excels in producing group-wise sparse and explainable

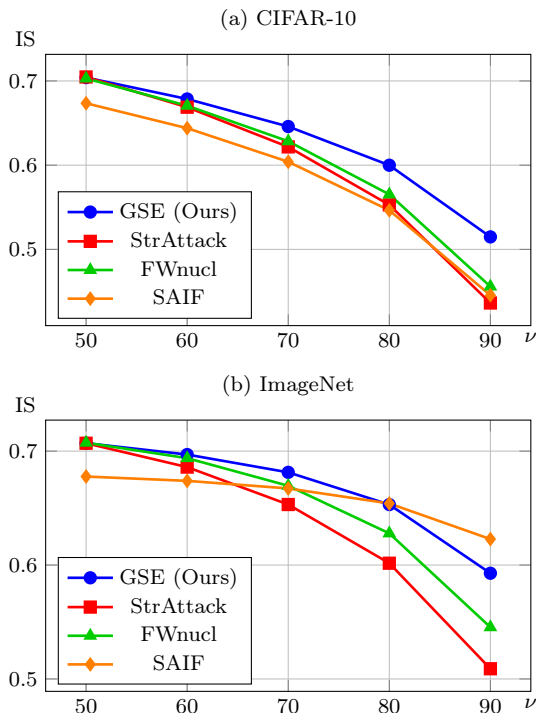


Figure 4: IS vs. percentile ν for targeted versions of our attack, StrAttack, FWnucl, and SAIF. Evaluated on a CIFAR-10 ResNet20 classifier (a), and an ImageNet VGG19 classifier (b).

adversarial perturbations, all while simultaneously

exhibiting the highest level of sparsity and the shortest computation time. Moreover, GSE excels over existing approaches in terms of quantitative metrics for interpretability and offers transparency for visualizing the vulnerabilities inherent in DNNs.

4.1 Social Impact

Adversarial attacks lay bare the vulnerability of DNNs. Our goal is to showcase the feasibility of crafting group-wise sparse and explainable adversarial attacks for natural images. This endeavour not only establishes a new benchmark for the research community to evaluate the robustness of deep learning algorithms but also suggests a simple defense strategy: employing the adversarial examples generated by GSE in adversarial training. For more sophisticated solutions, we advocate further exploration.

References

- [FW56] Marguerite Frank and Philip Wolfe. “An algorithm for quadratic programming”. In: *Naval Research Logistics Quarterly* 3 (1956).
- [Tyr70] R Tyrrell Rockafellar. “Convex analysis”. In: *Princeton mathematical series* 28 (1970).
- [Nes83] Yurii Nesterov. “A method for solving the convex programming problem with convergence rate $O(1/k^2)$ ”. In: *Proceedings of the USSR Academy of Sciences* 269 (1983).
- [KH+09] Alex Krizhevsky, Geoffrey Hinton, et al. “Learning multiple layers of features from tiny images”. In: *University of Toronto* (2009).
- [CSX13] Wenfei Cao, Jian Sun, and Zongben Xu. “Fast image deconvolution using closed-form thresholding formulas of l_q ($q=12, 23$) regularization”. In: *Journal of visual communication and image representation* 24.1 (2013), pp. 31–41.
- [LL15] Huan Li and Zhouchen Lin. “Accelerated proximal gradient methods for nonconvex programming”. In: *Advances in neural information processing systems*. 2015, pp. 379–387.
- [SZ15] Karen Simonyan and Andrew Zisserman. *Very Deep Convolutional Networks for Large-Scale Image Recognition*. 2015. arXiv: [1409.1556](https://arxiv.org/abs/1409.1556) [cs.CV].
- [He+16] Kaiming He et al. “Deep residual learning for image recognition”. In: *Proceedings of the IEEE conference on computer vision and pattern recognition*. 2016, pp. 770–778.
- [NK16] Nina Narodytska and Shiva Prasad Kasiviswanathan. “Simple Black-Box Adversarial Perturbations for Deep Networks”. In: *arXiv preprint arXiv:1612.06299* (2016).
- [Pap+16] Nicolas Papernot et al. “The limitations of deep learning in adversarial settings”. In: *2016 IEEE European symposium on security and privacy (EuroS&P)*. IEEE. 2016, pp. 372–387.
- [Zho+16] Bolei Zhou et al. “Learning deep features for discriminative localization”. In: *Proceedings of the IEEE conference on computer vision and pattern recognition*. 2016, pp. 2921–2929.
- [Bec17] Amir Beck. *First-order methods in optimization*. SIAM, 2017.
- [CW17] Nicholas Carlini and David Wagner. “Towards Evaluating the Robustness of Neural Networks”. In: *2017 IEEE symposium on security and privacy (sp)*. IEEE. 2017.
- [Ath+18] Anish Athalye et al. “Synthesizing robust adversarial examples”. In: *International conference on machine learning*. PMLR. 2018, pp. 284–293.
- [Mad+18] Aleksander Madry et al. “Towards deep learning models resistant to adversarial attacks.” In: *Proceedings of the International Conference on Learning Representations (ICLR)*. 2018.
- [CH19] Francesco Croce and Matthias Hein. “Sparse and imperceptible adversarial attacks”. In: *Proceedings of the IEEE/CVF International Conference on Computer Vision*. 2019, pp. 4724–4732.
- [INM19] Alexey Ignatiev, Nina Narodytska, and Joao Marques-Silva. “On relating explanations and adversarial examples”. In: *Advances in neural information processing systems* 32 (2019).

- [MMF19] Apostolos Modas, Seyed-Mohsen Moosavi-Dezfooli, and Pascal Frossard. “Sparsefool: A Few Pixels Make a Big Difference”. In: *Proceedings of the IEEE/CVF Conference on Computer Vision and Pattern Recognition*. 2019.
- [SHS19] David Stutz, Matthias Hein, and Bernt Schiele. “Disentangling adversarial robustness and generalization”. In: *Proceedings of the IEEE/CVF Conference on Computer Vision and Pattern Recognition*. 2019, pp. 6976–6987.
- [SVS19] Jiawei Su, Danilo Vasconcellos Vargas, and Kouichi Sakurai. “One pixel attack for fooling deep neural networks”. In: *IEEE Transactions on Evolutionary Computation* 23.5 (2019), pp. 828–841.
- [Xu+19] Kaidi Xu et al. “Structured adversarial attack: Towards general implementation and better interpretability”. In: *International Conference on Learning Representations*. 2019.
- [Fan+20] Yanbo Fan et al. “Sparse adversarial attack via perturbation factorization”. In: *Proceedings of European Conference on Computer Vision*. 2020.
- [Yan+20] Greg Yang et al. “Randomized smoothing of all shapes and sizes”. In: *International Conference on Machine Learning*. PMLR. 2020, pp. 10693–10705.
- [Zha+20] Jingfeng Zhang et al. “Attacks which do not kill training make adversarial learning stronger”. In: *International conference on machine learning*. PMLR. 2020, pp. 11278–11287.
- [Zho+20] Hang Zhou et al. “Lg-gan: Label guided adversarial network for flexible targeted attack of point cloud based deep networks”. In: *Proceedings of the IEEE/CVF Conference on Computer Vision and Pattern Recognition*. 2020, pp. 10356–10365.
- [WYD21] Hao Wang, Xiangyu Yang, and Xin Deng. “A Hybrid First-Order Method for Nonconvex ℓ_p -ball Constrained Optimization”. In: *arXiv preprint arXiv:2104.04400* (2021).
- [ZCW21] Mingkang Zhu, Tianlong Chen, and Zhangyang Wang. “Sparse and imperceptible adversarial attack via a homotopy algorithm”. In: *International Conference on Machine Learning*. PMLR. 2021, pp. 12868–12877.
- [Imt+22] Tooba Imtiaz et al. “SAIF: Sparse Adversarial and Interpretable Attack Framework”. In: *arXiv preprint arXiv:2212.07495* (2022).
- [KKW23] Ehsan Kazemi, Thomas Kerdreux, and Liqiang Wang. “Minimally Distorted Structured Adversarial Attacks”. In: *International Journal of Computer Vision* 131.1 (2023), pp. 160–176.